Biophysical Journal Volume 100 May 2011 2367–2377


# Effects of Conformational Peptide Probe DP4 on Bidirectional Signaling between DHPR and RyR1 Calcium Channels in Voltage-Clamped Skeletal Muscle Fibers

Rotimi O. Olojo,[†△] Erick O. Hernández-Ochoa,[†△] Noriaki Ikemoto,[‡] and Martin F. Schneider[†*]
[†]Department of Biochemistry and Molecular Biology, University of Maryland School of Medicine, Baltimore, Maryland; and [‡]Boston Biomedical Research Institute, Watertown, Massachusetts

ABSTRACT In skeletal muscle, excitation-contraction coupling involves the activation of dihydropyridine receptors (DHPR) and type-1 ryanodine receptors (RyR1) to produce depolarization-dependent sarcoplasmic reticulum $Ca^{2+}$ release via orthograde signaling. Another form of DHPR-RyR1 communication is retrograde signaling, in which RyRs modulate the gating of DHPR. DP4 (domain peptide 4), is a peptide corresponding to residues $Leu^{2442}$-$Pro^{2477}$ of the central domain of the RyR1 that produces RyR1 channel destabilization. Here we explore the effects of DP4 on orthograde excitation-contraction coupling and retrograde RyR1-DHPR signaling in isolated murine muscle fibers. Intracellular dialysis of DP4 increased the peak amplitude of $Ca^{2+}$ release during step depolarizations by 64% without affecting its voltage-dependence or kinetics, and also caused a similar increase in $Ca^{2+}$ release during an action potential waveform. DP4 did not modify either the amplitude or the voltage-dependence of the intramembrane charge movement. However, DP4 augmented DHPR $Ca^{2+}$ current density without affecting its voltage-dependence. Our results demonstrate that the conformational changes induced by DP4 regulate both orthograde E-C coupling and retrograde RyR1-DHPR signaling.

## INTRODUCTION

In skeletal muscle, depolarization of the transverse tubule system is detected by the dihydropyridine receptor (DHPR), a Cav1 $Ca^{2+}$ channel. Upon depolarization there is a reorientation of charged residues in transmembrane domains of DHPR that results in the activation of sarcoplasmic reticulum (SR) $Ca^{2+}$ release from the ryanodine receptor (RyR1) (1–4). The signal received by the RyR is recognized by a $Ca^{2+}$ conduction pathway located at the opposite side of the RyR. This sequential activation of DHPR and RyR1 to produce depolarization-dependent $Ca^{2+}$ release is known as orthograde signaling (5–7). Another form of DHPR-RyR1 communication is the retrograde signaling, in which RyRs modulate the gating of DHPR (8–11). In addition to this DHPR-RyR1 signaling, the RyR1 $Ca^{2+}$ release channel is subject to different forms of both extrinsic and intrinsic modulation. For instance, a variety of intracellular factors (such as $Ca^{2+}$, $Mg^{2+}$, calmodulin, and S100A1) extrinsically modulates the RyR1 activity (12–16).

The intrinsic modulation of opening/closing of the SR $Ca^{2+}$ release channels seems to be performed by global conformational changes of the RyR1 molecule, as indicated by high-resolution single particle analysis of cryo-electron microscopy images of RyR1 in its resting and activated states (17). Recent peptide probe studies of local conformational changes within the RyR1 have led to the hypothesis that the extent of interdomain interaction between an N-terminal domain and a central domain of RyR1 (designated as a domain switch) is involved in the channel regulation, thus playing an important role in the conformational regulation of RyR1 functions (18).

This hypothesis is consistent with the observations that domain peptide 4 (DP4), a decoy peptide corresponding to the $Leu^{2442}$-$Pro^{2477}$ region of the central domain, binds to the 51-kDa region including the N-terminus and activates the RyR1 channel (19). This suggests that there is an interdomain interaction between N-terminal domain and central domain, and that this interaction stabilizes the closed state of the channel. A variety of other observations is also consistent with this hypothesis (20–25). As is the case of increased sensitivity to caffeine or other agonists in malignant hyperthermia (MH) (26–30), DP4 (30–100 $\mu$M) was also found to increase the sensitivity to caffeine for channel activation (22).

Previous work in skeletal muscle has also shown that DP4 enhanced force response to submaximal depolarization by ionic substitution in mechanically skinned fibers (31) and increased the frequency of $Ca^{2+}$ sparks in permeabilized amphibian fibers (23). However, the influence of DP4 on voltage-clamp depolarization-evoked $Ca^{2+}$ release has not been evaluated. In this work, we sought to explore effects of DP4 on orthograde excitation-contraction (E-C) coupling and retrograde RyR1-DHPR signaling in whole-cell, voltage-clamped adult murine skeletal muscle fibers.

## MATERIALS AND METHODS

### Ethical approval

All animals were housed in a pathogen-free area at the University of Maryland, Baltimore. The animals were euthanized according to authorized

*Submitted August 7, 2010, and accepted for publication April 4, 2011.*

[△]Rotimi O. Olojo and Erick O. Hernández-Ochoa contributed equally to this work.

*Correspondence: mschneid@umaryland.edu

Editor: Michael Pusch.


0006-3495/11/05/2367/11 $2.00

doi: 10.1016/j.bpj.2011.04.012

procedures of the Institutional Animal Care and Use Committee, University of Maryland, Baltimore.

## FDB fiber preparation

Fibers were prepared using enzymatic dissociation of FDB muscles of 6–7-week-old C57BL mice, and were cultured as previously described (32).

## Peptide synthesis

The amino-acid sequence of the synthetic peptides corresponding to the selected subdomains of RyR1 DP4 is

2442LIQAGKGEALRIRAIL***R***
SLVPLDDLVGIISLPLQIP2477

and Mutant DP4 is

2442LIQAGKGEALRIRAIL***C***
SLVPLDDLVGIISLPLQIP2477

with **R**2458**C** substitution were synthesized as previously described (22–24).

## Solutions

Whole-cell $Ca^{2+}$ current and charge movement measurements were carried out as previously described (33). The standard pipette solution (internal) contained: 140 mM Cs-CH3SO3, 10 mM HEPES, 20 mM EGTA, 6 mM MgCl2, 11.5 mM CaCl2, 4 mM Na2ATP, 14 mM creatine phosphate, 0.3 mM Na2GTP, and 0.1 mM leupeptin and solution pH adjusted to 7.4 with CsOH to obtain a buffered solution. Fibers were dialyzed via the patch pipette with 50–75 $\mu$M fluo-4 5 $K^+$. Where noted, 50–100 $\mu$M DP4 or mutant DP4 was also included in the internal solution. Fibers were dialyzed for exactly 20 min before the start of data acquisition.

## Electrophysiology and data analysis

Membrane current measurements were performed using the whole-cell configuration of the patch-clamp technique (34) with modifications for mammalian FDB fibers detailed elsewhere (33,35). For results shown later in Fig. 6, *A–D*, a muscle action potential was recorded in current clamp mode and then used as the command voltage (36).

## Fluo-4 high-speed line-scan (*x-t*) confocal microscopy

Fluo-4 fluorescence measurements were carried out on an LSM 5 Live system (Carl Zeiss, Jena, Germany) as previously described (37). Average intensity of fluorescence as a function of time ($F(x,t)$) within a selected segment of the scan line within a fiber was measured using Image Examiner (Carl Zeiss). The average $F_0$ value in each line segment before test pulse is used to scale fluo4 fluorescence in the same region as $F/F_0$.

## Time course of free $Ca^{2+}$ concentration

Free $Ca^{2+}$ was calculated from the $F/F_0$ record by correcting for kinetic lag and dye saturation using an approach previously described (38) but adapted here for $F/F_0$ records (see (39)). Under conditions when the dye is not at equilibrium with the cytosolic free $Ca^{2+}$, the time course of cytosolic free $Ca^{2+}$concentration ($[Ca]cyto(t)$), is given by

$$[Ca]_{cyto}(t) = KD_d\{(1/koff_d)\,dF(t)/dt + F(t) - F_{min}\}/\{F_{max} - F(t)\} \quad (1)$$

(see (38), Eq. 5, with rearrangements), where $KD_d$ is the dissociation constant for $Ca^{2+}$ from the indicator dye, $koff_d$ is the off rate constant for $Ca^{2+}$ dissociation from the dye, $F$ is the fiber fluo-4 fluorescence signal and $F_{max}$ and $F_{min}$ are the fluorescence at saturating and zero free $Ca^{2+}$, respectively.

When the concentration is changing slowly, the following condition applies:

$$[Ca] \approx KD_d\{(F - F_{min})/(F_{max} - F)\}. \quad (2)$$

Then, average $[Ca^{2+}]cyt\ (t)$ is derived from $F(t)/F_0$ (39) as

$$[Ca_{2+}]_{cyto}(t) = [Ca_{2+}]_{cyto(0)}\{(F(t)/F_0) + (1/koff_d)\,d(F(t)/F_0)/dt\}, \quad (3)$$

where $[Ca^{2+}]cyto(0)$ is free cytosolic $[Ca^{2+}]$ at resting levels. This equation assumes that the dye is far from saturation by $Ca^{2+}$, which appears justified for fluo-4 considering that $[Ca^{2+}]cyto$ was always much lower than the value of fluo-4's *KD* previously determined using in situ calibrations (37). $[Ca^{2+}]cyto(0)$ was set equal to 0.081 $\mu$M, the average value measured in parallel studies using indo-1 in voltage-clamped FDB fibers with and without 50 $\mu$M DP4. If we use the nonsignificantly different mean resting $[Ca^{2+}]$ of 75 and 86 nM for control and DP4-dialyzed fibers, respectively, the calculated percent increase in peak $Ca^{2+}$ release flux induced by DP4 for pulses to +20 mV would be 6% larger than presented here.

## Calculation of $Ca^{2+}$ release flux

### *Time course of the rate of change of [Ca-EGTA]*

Under the conditions of 20 mM EGTA with added $Ca^{2+}$ in the pipette, EGTA is still the major binding site for released $Ca^{2+}$. In that case $d\,[Ca\text{-}EGTA](t)/dt$ provides a good approximation to the rate of SR Ca release in the fiber, and will be used in the $Ca^{2+}$ release calculations presented here. For $Ca^{2+}$ binding to EGTA,

$$d[Ca\text{ - }EGTA](t)/dt = kon_e[Ca](t)[EGTA](t) - koff_e[Ca\text{ - }EGTA](t), \quad (4)$$

where $kon_e$ and $koff_e$ are on- and off-rate constants for $Ca^{2+}$ binding to EGTA. Because

$$[EGTA](t) = [EGTA]_{tot} - [Ca\text{ - }EGTA](t),$$

$$d[Ca\text{ - }EGTA](t)/dt = kon_e[Ca](t)\{[EGTA]_{tot} - [Ca\text{ - }EGTA](t)\} - koff_e[Ca\text{ - }EGTA](t). \quad (5)$$

Equation 5 was solved numerically using $[Ca^{2+}]cyto(t)$ from Eq. 3, and using the Euler method to calculate the time course of $d[Ca\text{-}EGTA](t)/dt$, which was used as the time course of the rate of $Ca^{2+}$ release from the SR during the voltage-clamp pulses. $[EGTA]_{tot}$ in the fiber was assumed to be 70% of that in the pipette solution. $[EGTA]$ and $[Ca\text{-}EGTA]$ inside the fiber at the start of each pulse were calculated from $[EGTA]/[Ca\text{-}EGTA] = KD_e/[Ca^{2+}]$ and from the conservation of total EGTA. The parameter values used in our calculations were $koff_d = 90\ s^{-1}$ (40), $kon_e = 15\ (\mu M\ s)^{-1}$ (39) and $koff_e = 1.2\ s^{-1}$ (EGTA $KD = 0.08\ \mu M$).

## Statistical analysis

All statistical analysis was performed using ORIGINPro 8.0 (http://www.originlab.com/). All data are presented as mean ± SE unless otherwise

noted. Statistical significance was assessed using either parametric two sample *t*-test or with the nonparametric Mann-Whitney rank-sum test. Significance was set at $P < 0.05$.

## RESULTS

### Depolarization-evoked fluo-4 fluorescence signals in a control and in a DP4-dialyzed fiber

The first series of experiments aimed to evaluate the effects of DP4 on DHPR to RYR communication (i.e., orthograde signaling). Fig. 1 illustrates the protocol used for monitoring $Ca^{2+}$ transients in these studies. FDB muscle fibers isolated from C57BL mice were voltage-clamped at a holding potential of −80 mV. In these experiments, 50 $\mu$M fluo-4 was included in the patch pipette solution, and was allowed to diffuse into the fiber for exactly 20 min after seal formation and before starting data acquisition. A bracketing set of pulses to −20 mV was applied before and after each pair of pulses to another voltage to monitor stability of the fiber. Fig. 1 shows raw fluo-4 fluorescence $Ca^{2+}$ transients obtained from a control fiber (Fig. 1 *A*) and from a DP4-dialyzed fiber (Fig. 1 *B*) using series of 80-ms voltage-clamp step depolarizations increasing in amplitude by 20 mV, with a 30-s interval between pulse applications. The 20-min time interval for diffusion of pipette solution into the fiber before starting data acquisition and the 30-s interval between applications of successive pulses were strictly adhered to in all experiments. Confocal line-scan images were acquired at 50 or 100 $\mu$s/line synchronized to start 300 ms before each of the pulses during step depolarizations.

Using the voltage protocol illustrated in Fig. 1 *C*, a detectable fluo-4 fluorescence change was typically first detected in most fibers with pulses to above −40 mV, and saturated with pulses to ~+20 mV. It was observed that the resting fluorescence ($F_0$) increased during the course of the successive pulse applications, leading to increased baseline $F_0$ values as shown in Fig. 1, *D* and *E*. The resting fluorescence before starting the application of successive depolarizing pulses is marked as $F_0(-20,\text{start})$ and the background fluorescence $F_b$ (set to zero by background subtraction) are as illustrated in Fig. 1, *D* and *E*. The amplitude of the $\Delta F$ signal for the repeated pulses to −20 mV appears to be changing with time and/or with the intervening pulses and the accompanying successive $Ca^{2+}$ release and uptake. The value of $F_0$ was continuously increasing with time over the course of each experiment. In view of the strong $Ca^{2+}$ buffering by EGTA in these experiments, we believe that the increasing $F_0$ was due to increasing entry of fluo-4/EGTA during the course of the experiment rather than to an increase in resting [$Ca^{2+}$] (see below). In any case, careful examination of the changes in both $F_0$ and $\Delta F$ indicated that both were changing over the course of the experiment (see Fig. S1 in the Supporting Material).

### Resting [$Ca^{2+}$] in control and DP4 dialyzed fibers

To experimentally determine the resting [$Ca^{2+}$] under the conditions of our experiments, we carried out a parallel set of experiments using indo-1 in the pipette instead of fluo-4, with all other constituents being the same (see additional Materials and Methods in the Supporting Material). The indo-1 fluorescence emission ratio did not change significantly with time starting 20 min after whole-cell configuration establishment (Fig. S2 *C*), although the absolute fluorescence did (Fig. S2 *D*), indicating continued indo-1 entry. Furthermore, the indo-1 fluorescence ratio, and the free [$Ca^{2+}$] calculated from it were not significantly

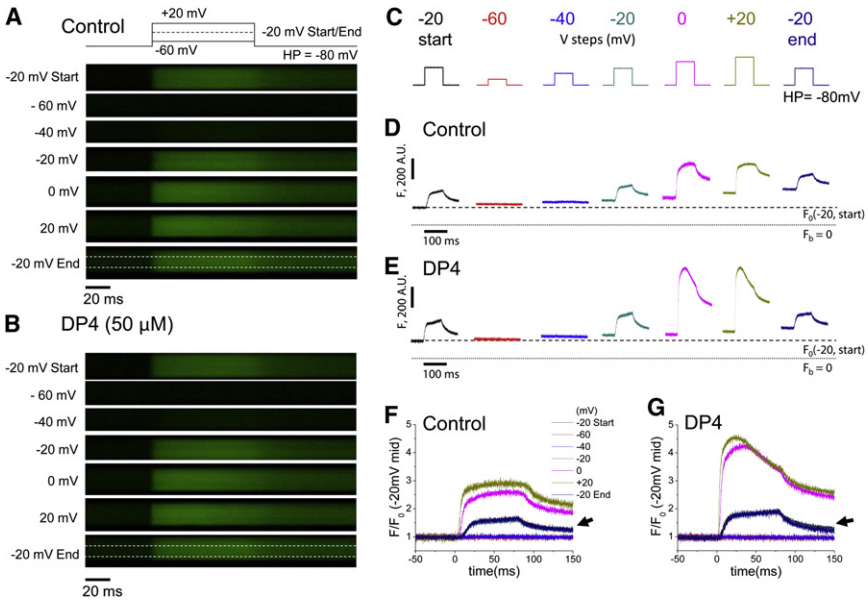


FIGURE 1 Depolarization-evoked fluo-4 $Ca^{2+}$ transients in a control fiber and in another fiber studied with 50 $\mu$M DP4 in the internal solution. (*A*, *open box*) Region of interest drawn in the center of the fiber that was used to measure fluorescence intensity. (*B*) Representative confocal line scan (*x-t*) fluo4 images synchronized with the voltage-clamp protocol, consisting of 80-ms depolarizing steps from a holding potential of −80 mV to the voltages indicated next to the images, from a fiber dialyzed with the standard control internal solution (*A*) or from a different fiber dialyzed with a DP4-containing internal solution. (*C*) Voltage protocol. (*D* and *E*) Time course of fluo-4 fluorescence obtained from panels *A* and *B*. (*F* and *G*) Superimposed $F/F_0$ traces empirically corrected (see Results), relative to −20 mV depolarization in the middle of the protocol for a control and a DP4-dialyzed fiber, respectively. (*Arrows*) Superimposed traces obtained with the pulses at −20 mV.

different with or without DP4 (50 $\mu$M) in the pipette solution (Fig. S2, *A* and *B*). These results provide strong support for the interpretation that the resting free [$Ca^{2+}$] is fully controlled by the EGTA buffer at a constant level throughout each of our experiments, which began at 20 min after seal formation. It then continued for, at most, another 7 or 8 min, and the resting free [$Ca^{2+}$] level was not significantly different with or without DP4 (86 nM vs. 75 nM, respectively; $P > 0.05$). Thus, the increase in resting fluorescence with time in the experiments using fluo-4 appears to be the result of increasing concentration of the fluo4 rather than a change in free [$Ca^{2+}$].

### Empirical correction for changes during dye entry

To compensate for possible changes in the fiber with time during application of the pulse sequence in Fig. 1, regardless of the mechanism involved, we used the records for the repeated pulses to −20 mV in each fiber to calculate model-independent empirical compensation factors. $\Delta F/F_0$ was calculated for each pulse in the sequence in each fiber. The $\Delta F/F_0$ records for the pulses to −20 mV at the start and end of the sequence were scaled to the $\Delta F/F_0$ record for the pulse to −20 mV in the middle of the sequence. The scaled records showed excellent agreement (records marked by *arrows* in Fig. 1, *F* and *G*; three records superimposed). The intervening pulses (to −60 and −40 mV between the start- and mid-pulse to −20 mV, and the pulses to 0 and +20 mV between the mid- and end-pulse to −20 mV) were scaled by one- or two-thirds of the scale factor for the bracketing pulses to −20 mV in each fiber, giving the other records in Fig. 1, *F* and *G*. Such scaled records were then represented as $F/F_0$ relative to the middle −20 mV pulses and used for all further calculations for each fiber.

### DP4 potentiates fluorescence signals, free $Ca^{2+}$, and $Ca^{2+}$ release flux in DP4-dialyzed FDB fibers

Fig. 2 shows an averaged time course of fluo-4 $Ca^{2+}$ transients elicited by 80-ms step depolarization and expressed as $F/F_0$ obtained from control (Fig. 2 *A*, $N = 5$) and 50 $\mu$M DP4-dilayzed fibers (Fig. 2 *D*, $N = 5$) both with application of an initial and final voltage pulse to −20 mV and a series of pulse voltages in between from −60 mV to +20 mV at 20 mV step increments, as shown in Fig. 1.

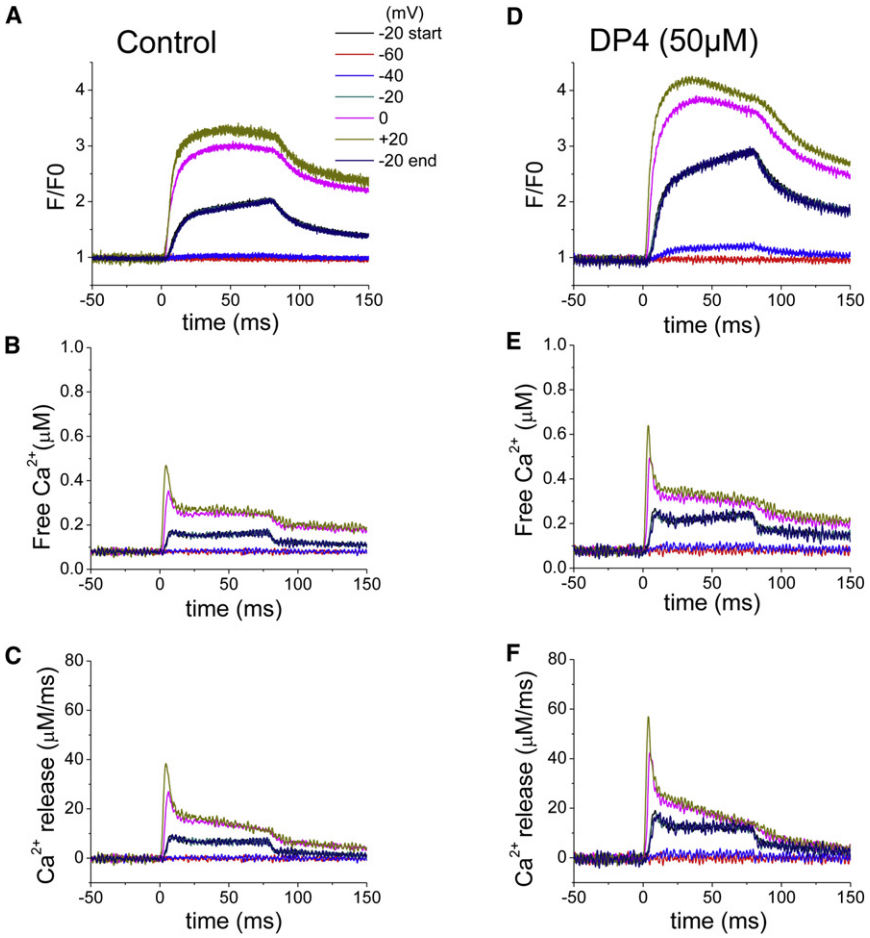


FIGURE 2 Fluo-4 fluorescence transients, free [$Ca^{2+}$] and $Ca^{2+}$ release flux from control and DP4-dialyzed fibers. Average ($N = 5$) fluo-4 $\Delta F/F_0$ records expanded in time using pulse protocol shown in Fig. 1 from control (*A*) and from 50 $\mu$M DP4 dialyzed fibers (*D*). (*B* and *E*) Free [$Ca^{2+}$] waveforms derived from panels *A* and *D* calculated using Eq. 3 (see Materials and Methods). (*C* and *F*) $Ca^{2+}$ release flux, calculated from Eq. 5. Comparison of the two sets of data show potentiation of $Ca^{2+}$ signals by addition of DP4.

The correction for possible changes in the fiber over the course of each experiment described above was applied to give the presented $F/F_0$ records (Fig. 2, *A* and *D*), and such records were used to calculate the free cytosolic $Ca^{2+}$ concentration (free $[Ca^{2+}]$). The estimation of the $Ca^{2+}$ release flux in each fiber was then calculated from its free $Ca^{2+}$ waveform.

For each fiber, Eq. 3 was used to calculate average cytosolic free $[Ca^{2+}]$, whereas the rate of $Ca^{2+}$ release from the inside of the SR into the cytosol was calculated using Eq. 5 (see additional Materials and Methods in the Supporting Material). Fig. 2, *B* and *C*, on the left presents the average of the records of free $[Ca^{2+}]$ and $Ca^{2+}$ release flux from five fibers for the control measurements, whereas corresponding data on the right (Fig. 2, *E* and *F*) are the averages from five fibers dialyzed with 50 $\mu$M DP4. DP4 increased the average fluo-4 signal at each voltage, and increased the calculated free $Ca^{2+}$ as well as the magnitude of the peak $Ca^{2+}$ release (peak $Ca^{2+}$ release at +20 mV for control fibers = 38.4 ± 7.7 $\mu$M ms$^{-1}$ vs. 56.9 ± 10.2 $\mu$M ms$^{-1}$ for DP4-dialyzed fibers; $n = 5$, $P < 0.05$).

In another series of experiments (Fig. 3), fibers were dialyzed with 100 $\mu$M DP4, or with 100 $\mu$M of DP4 mutated at residue 2458 (***R***2458***C*** substitution; hereafter referred to as Mut-DP4), or with control internal solution without any DP4 or Mut-DP4. Here the pulse sequence for the first half of the experiment was identical to that in Figs. 1 and 2, but was followed by another sequence of pulses ranging from +10 to −50 mV of decreasing amplitude in 20 mV increments, with a reference pulse to −20 mV at the start, middle, and end of the sequence. Correction for changes with time was identical to that used for the first sequence. The second sequence was then normalized to the first by scaling all records in the second sequence by the ratio of the $\Delta F/F_0$ values for the middle pulse, to −20 in the first sequence, to that in the second sequence.

Fig. 3 presents averages of $Ca^{2+}$ release flux profiles obtained from four control fibers (Fig. 3 *A*), four fibers dialyzed with 100 $\mu$M DP4 (Fig. 3 *B*), or four fibers dialyzed with 100 $\mu$M Mut-DP4 (Fig. 3 *C*). The dialysis of 100 $\mu$M DP4 further enhanced the peak $Ca^{2+}$ release rates when compared to 50 $\mu$M DP4 described in earlier experiments (Fig. 2), whereas the 100 $\mu$M Mut-DP4 produced peak values similar to the control. The records for the repeated pulses to −20 mV are shown in green. Comparison of the three panels shows elevation of $Ca^{2+}$ release flux at intermediate and extreme positive voltages in the presence of 100 $\mu$M DP4.

Using data obtained from each of the fibers used in Fig. 3, *A*–*C*, average values of the peak release rate were calculated and plotted as a function of voltage (*R-V* profiles in Fig. 3 *D*). The data were fitted to a single Boltzmann function described by the equation (37)

$$R(V) = R_{max}/\left(1+\exp\left(\left(V_{half}-V\right)/k\right)\right), \qquad (6)$$

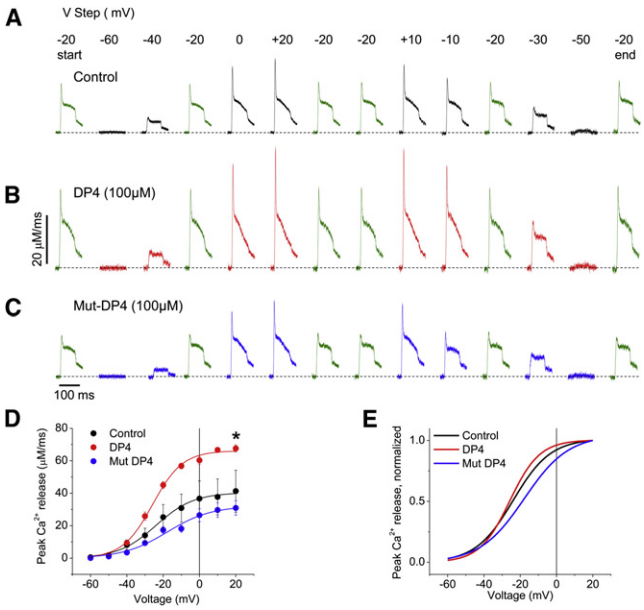


FIGURE 3 DP4 at 100 $\mu$M potentiates voltage-dependent $Ca^{2+}$ release flux. Time course of the averaged $Ca^{2+}$ release flux for control (*A*), 100 $\mu$M DP4-dialyzed fibers (*B*), and 100 $\mu$M Mut-DP4-dialyzed fibers (*C*) in response to test depolarizations indicated (*top* of figure). (*Green*) $Ca^{2+}$ release records for the repeated pulses to −20 mV. Addition of 100 $\mu$M DP4 potentiates the amplitude of $Ca^{2+}$ release flux. $Ca^{2+}$ release flux was calculated from Eq. 5. (*D*) Average peak release records plotted versus voltage (R-*V*) relationships for Mut-DP4 (*blue symbols*), control (*black symbols*), and 100 $\mu$M DP4-dialyzed fibers (*red symbols*). Continuous lines through the symbols are best fits to a single Boltzmann function from Eq. 6 (see Results). (*E*) Normalized peak $Ca^{2+}$ release versus voltage, showing that DP4 dialysis does not change the $V_{half}$ of the *R-V* relationship when compared to the control counterpart. These results reveal a significant 64% enhancement ($N = 4$; * $P < 0.05$) in $R_{max}$ induced by 100 $\mu$M DP4.

where $R_{max}$ is the maximum release rate, $V_{half}$ defines the potential when $R = 0.5\ R_{max}$, and $1/k$ is a measure of the steepness of the *R-V* relationship. Average ± SE for $R_{max}$, $V_{half}$, and $k$ parameters were: 32.1 ± 2.2 $\mu$M ms$^{-1}$, −18 ± 2.8 mV, and 12.1 ± 2 mV; 40.3 ± 1.2 $\mu$M ms$^{-1}$, −24 ± 1.2 mV, and 10.3 ± 1 mV; and 66.1 ± 1.2 $\mu$M ms$^{-1}$, −26 ± 0.7 mV, and 8.2 ± 0.6 mV for Mut-DP4, control, and DP4-dialyzed fibers, respectively. This analysis reveals a significant 64% enhancement ($N = 4$; $P < 0.05$) in the maximum peak $Ca^{2+}$ release with the addition of 100 $\mu$M DP4 when compared to the control fibers. Fig. 3 *E* plots the *R-V* curves normalized to $R_{max}$, allowing a better visualization of the effects of DP4 on the voltage dependence and steepness of the $Ca^{2+}$ release. The $V_{half}$ values shown here indicate a nonsignificant change in the voltage-dependence of $Ca^{2+}$ release arising from addition of DP4 (Fig. 3, *D* and *E*). The mutant-DP4 did not produce a significant change in the amplitude of the $Ca^{2+}$ release ($P > 0.05$).

To evaluate the kinetic effect of the addition of 100 $\mu$M DP4, $Ca^{2+}$ release flux profiles for control and 100 $\mu$M DP4-dialyzed fibers were plotted together and normalized

to the peak values for selected voltages that elicited $Ca^{2+}$ release, i.e., −20 mV, −10 mV, 0 mV, and +20 mV (Fig. 4, *A–D*). The insets show expanded timescale plots of the same records. Each of the $Ca^{2+}$ release waveforms is characterized by a pronounced early peak that occurs within 10 ms of the application of these larger pulse depolarizations. This is then followed by an initial rapid decline and a much slower decline with time in a profile that is believed to reflect an early partial inactivation of the RyR1 and the later effect of a time-dependent decline of the SR $Ca^{2+}$ content, respectively (41,42). The kinetics of the peak formation and the initial decline appear unchanged by DP4 from the overlay of the normalized $Ca^{2+}$ release peak (Fig. 4, *A–D*). Intermediate and large depolarizations produced a relatively faster decline of the slower component of the $Ca^{2+}$ release, which may be attributed to enhanced decline of the SR $Ca^{2+}$ content.

It has been suggested that the affinity of EGTA may be lower in the fiber interior than in free solution (39). A reduction in effective value of *KD* has been demonstrated directly for the EGTA-based fluo-3 and is attributed to its binding to intracellular proteins and its engaging in multimolecular reactions (43), a complication due to the intracellular environment (44). We therefore examined the effect on our analysis of assuming a lower EGTA affinity in the fiber by changing $koff_e$ from 1.2 to 7.5, corresponding to an increase in EGTA *KD* from 0.08 to 0.5 $\mu$M. When we made this change in parameter values, the absolute amplitude of the peak release was increased by 74% with DP4 and by 72% without DP4 (see Fig. S3, *A* and *B*), giving essentially the same relative effect of DP4 (46% enhancement) for either calculation of peak release (see *insets* in Fig. S3, *A* and *B*). Furthermore, the early time courses of normalized release flux for the calculations with the two values of $koff_e$ were entirely unaffected, and only a very minor change in time course was produced in the late phase of release by changing $koff_e$ (see Fig. S3, *C* and *D*). Thus, our calculations are very insensitive to the $Ca^{2+}$ affinity used for EGTA in the fiber.

## Nonlinear charge movement currents are unchanged with addition of DP4

We also evaluated charge movement parameters in fibers dialyzed with 75 $\mu$M DP4 (see Fig. S4), and found no

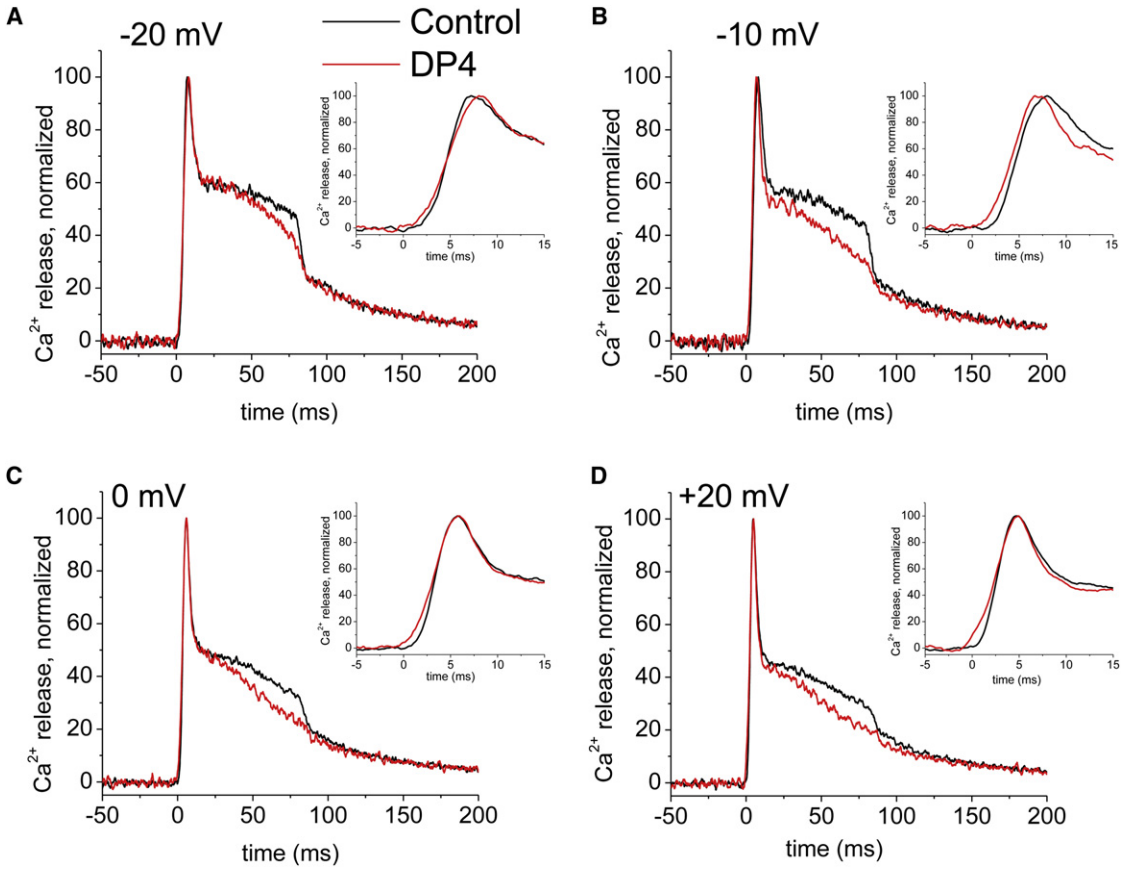


FIGURE 4 Control and DP4-dialyzed fibers demonstrate almost identical relative time courses of $Ca^{2+}$ release. Normalized $Ca^{2+}$ release versus time was analyzed at −20 (*A*), −10 (*B*), 0 (*C*), and +20 mV (*D*), in both the control and DP4-dialyzed fibers to evaluate the kinetic effect of 100 $\mu$M DP4. (*Insets*) Zoom-in versions of the rising phase of $Ca^{2+}$ release and the comparison of plots from control and DP4-dialyzed fibers. The rising phase and the initial decline of $Ca^{2+}$ release appear to be minimally affected in DP4-dialyzed fibers.

significant changes in kinetics, amount, midpoint voltage, or steepness of voltage dependence of charge movement in DP4-dilayzed fibers when compared to control counterparts ($P > 0.05$, $N = 5$).

## Whole cell $Ca^{2+}$ channel current is enhanced with dialysis of DP4

We next examined whether DP4 also caused changes in RyR1 to DHPR communication (i.e., retrograde signaling). To this end, we measured whole-cell $Ca^{2+}$ currents generated by the DHPR in control and in DP4-dialyzed fibers. Fig. 5 *A* shows representative macroscopic $Ca^{2+}$ current traces from a control (*black trace*), Mut-DP4-dialyzed (*blue trace*, 100 $\mu$M), and DP4-dialyzed fibers (*red trace*, 100 $\mu$M) using step depolarizations lasting 80 ms applied from a holding potential of $-80$ mV. Traces shown were obtained at 0 mV where the maximum inward amplitude occurred during step depolarizations. Fig. 5 *B* shows the average peak $Ca^{2+}$ current density plotted against voltage (*I-V*) from control (*black circles*), Mut-DP4 (*blue circles*), and DP4-treated fibers (*red circles*). Addition of 100 $\mu$M DP4 induced ~47% enhancement of the peak inward $Ca^{2+}$ current density as illustrated in Fig. 5 *B*. The solid lines through the *I-V* curves in Fig. 5 *B* are least-squares fits of the data to a modified Boltzmann-Ohmic equation (8,33),

$$I = G_{max}(V - V_{rev})/\left[1 + \exp\left(-\left(V - V_{half}\right)/k\right)\right], \quad (7)$$

where $G_{max}$ is the maximum conductance, $V$ is the membrane potential, $V_{rev}$ is the reversal potential, $V_{half}$ is the half-activation potential, and $k$ is a measure of the steepness. Average parameter values from $G_{max}$, $V_h$, $k$, and $V_{rev}$ for control fibers were: 157.0 $\pm$ 0.2 pA/mV, $-11.1$ $\pm$ 0.7 mV, 3.4 $\pm$ 0.5 mV, and 42 $\pm$ 4 mV. The corresponding sets of values for the Mut- DP4 were: 139.3 $\pm$ 0.2 pA/mV, $-11.4$ $\pm$ 0.8 mV, 3.7 $\pm$ 0.5 mV, and 48 $\pm$ 6 mV, whereas values corresponding to DP4 were 195.3 $\pm$ 0.3 pA/mV, $-10.4$ $\pm$ 0.6 mV, 2.8 $\pm$ 0.8 mV, and 49 $\pm$ 7 mV. These parameters were used to obtain voltage dependence of $Ca^{2+}$ conductance for the control, Mut-DP4, and DP4 fibers (Fig. 5 *C*).

DP4 induced a significant 24% enhancement on $G_{max}$ ($P < 0.05$, $N = 8$) whereas Mut-DP4 did not cause any significant change in the properties of whole-cell $Ca^{2+}$ current. We concluded that the enhancement of the $Ca^{2+}$ current caused by addition of DP4 is voltage-independent, judging by the negligible effects on both $V_{half}$ and $k$ Boltzmann's parameters of the $Ca^{2+}$ channel conductance.

## DP4 potentiates action-potential induced $Ca^{2+}$ transients in skeletal muscle FDB fibers

One additional and interesting finding of an earlier report was that DP4 did not significantly alter the size of the twitch response elicited by action potential (AP) stimulation in mechanically peeled fibers (31). To address whether DP4

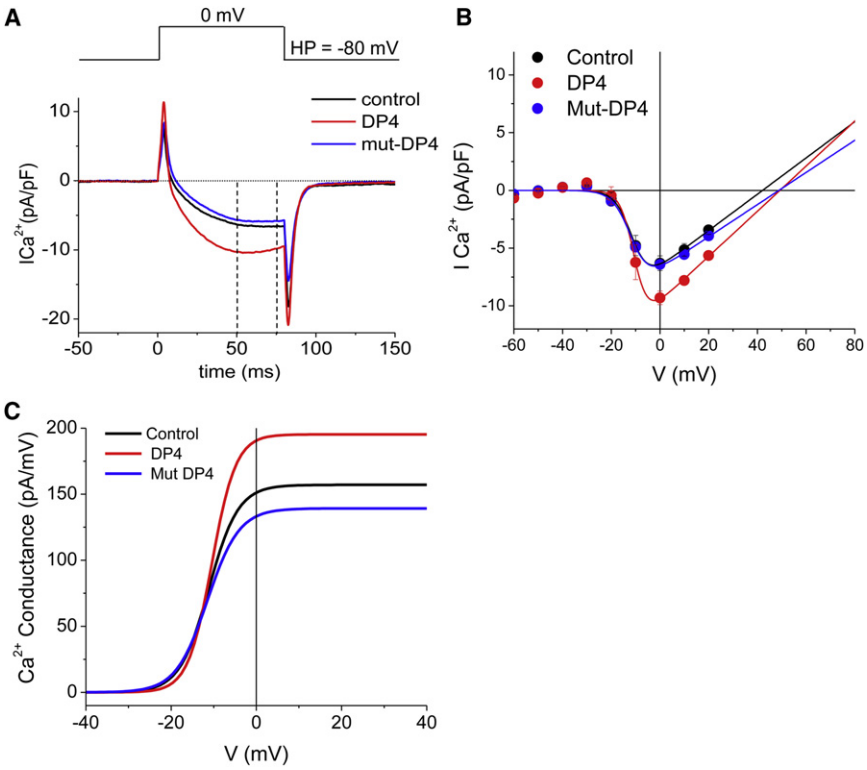


FIGURE 5 Intracellular dialysis of DP4 enhances macroscopic $Ca^{2+}$ current in FDB fibers. (*A*) Representative macroscopic $Ca^{2+}$ current traces from 100 $\mu$M Mut-DP4-dialyzed (*blue trace*), control (*black trace*), and 100 $\mu$M DP4-dialyzed fibers (*red trace*) elicited by a test depolarization to 0 mV. Macroscopic currents were elicited by 80-ms depolarizing pulses using 2 mM $Ca^{2+}$ as the charge carrier. (*Vertical dashed lines*) Time used to measure average current density values to create I-V plots. (*B*) I-V relationships of average data from Mut-DP4-dialyzed (*blue symbols*), control (*black symbols*), and DP4-dialyzed fibers (*red symbols*). The solid lines through the I-V profiles in panel *B* are least-squares fits of the data to a modified Boltzmann-Ohmic equation, Eq. 7 (see Results). (*C*) $Ca^{2+}$ conductance versus voltage (*GCa-V*) relationship of Mut-DP4, control, and DP4-dilayzed fibers derived from Eq. 7. These results indicate that DP4 induced a significant 24% enhancement on $G_{max}$ ($N = 8$; $P < 0.05$).

enhances AP-evoked $Ca^{2+}$ release in fibers with intact sarcolemma and open transverse tubules, we voltage-clamped fibers using the AP waveform (Fig. 6 *A*), interspersed with depolarizing pulses to −20 mV (see Fig. S5). The averaged AP evoked $Ca^{2+}$ transients measured in control (*black trace*; $n = 5$) and DP4-dialyzed fibers (*red trace*, $n = 5$) in Fig. 6 *B* show that DP4 (100 $\mu$M) enhanced the AP evoked $Ca^{2+}$ transients as measured by $F/F_0$ values.

Fig. 6 *C* shows time course of calculated free [$Ca^{2+}$] obtained from Eq. 3, demonstrating a 57% enhancement of peak free [$Ca^{2+}$] during an AP voltage-clamp when fibers were dialyzed with 100 $\mu$M DP4. Similarly, the $Ca^{2+}$ release flux calculated from Eq. 5 shows 68% potentiation of the AP-evoked $Ca^{2+}$ release upon addition of DP4 as illustrated in Fig. 6 *D* (control peak $Ca^{2+}$ release flux ($\mu$M ms$^{-1}$) = 48 vs. 81 for DP4 dialyzed fibers; $N = 5$, $P < 0.05$). For comparison, $Ca^{2+}$ transients and the corresponding time course of free [$Ca^{2+}$] and $Ca^{2+}$ release elicited by a 80-ms depolarizing pulse to −20 mV in the same fibers is illustrated in Fig. 6, *E–H*. The above results indicate that DP4 enhances $Ca^{2+}$ release, both for voltage-clamp pulses and for the voltage-clamp-imposed AP command.

## DISCUSSION

This report describes the effects of the DP4 peptide on depolarization-induced global SR $Ca^{2+}$ release detected by ultra high-speed laser confocal microscopy in whole-cell voltage-clamped adult FDB skeletal muscle fibers. DP4 is a domain peptide corresponding to the Leu$^{2442}$-Pro$^{2477}$ region of the RyR1 central domain (21). Interaction of DP4 with its complimentary domain within the RyR1 interferes with normal intrachannel domain-domain interaction that is hypothesized to play a key role in stabilizing one of the closed states of the channel (24). Thus the peptide is believed to unzip the interacting N-terminal and central domains (18,21,22,25), to

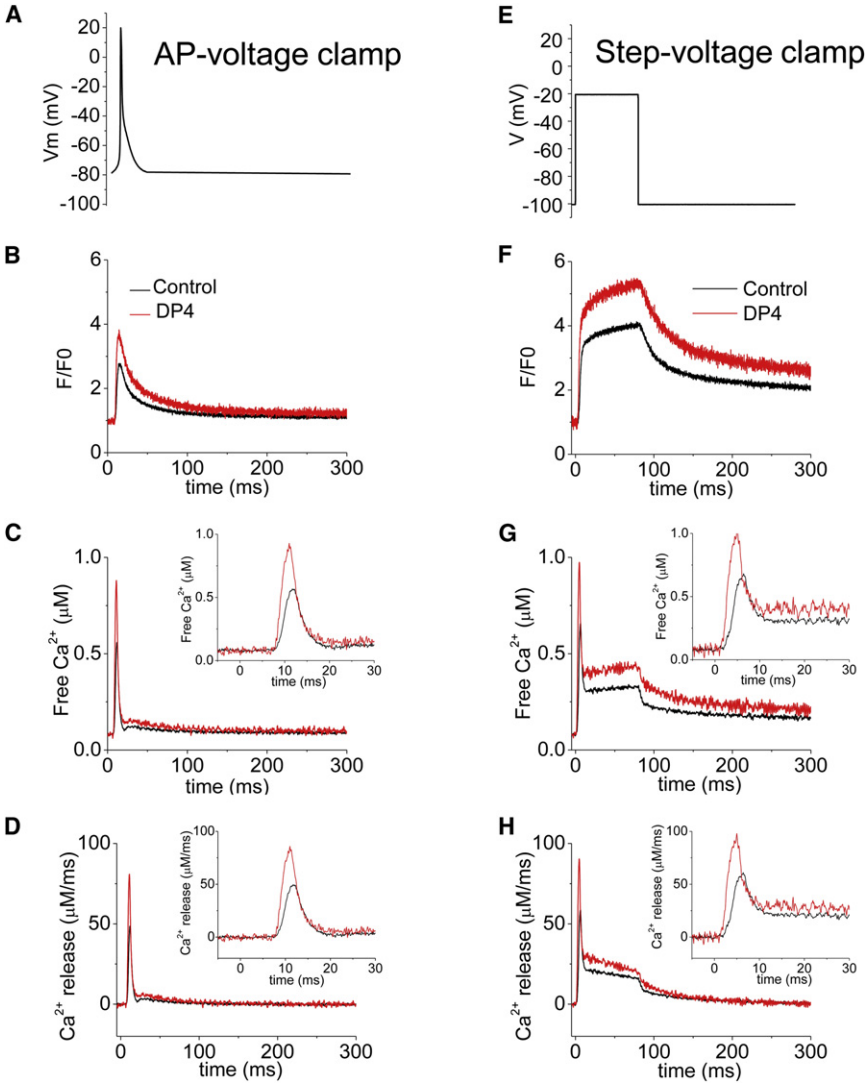


FIGURE 6 DP4 enhances AP-evoked $Ca^{2+}$ transients and $Ca^{2+}$ release. AP waveform (*A*) or 80-ms step depolarization (*E*) used to evaluate the effect of DP4. Time course of $F/F_0$ obtained from control fibers (*black trace*) and from 100 $\mu$M DP4-dialyzed fibers (*red traces*) using AP waveform (*B*) or step depolarization (*F*). (*C* and *G*) Free [$Ca^{2+}$] waveforms derived from panels *B* and *F* calculated using Eq. 3 (see Materials and Methods). (*D* and *H*) $Ca^{2+}$ release flux, calculated from Eq. 5. (*Insets*) Zoom-in versions of the rising phase of $Ca^{2+}$ release from control and DP4-dialyzed fibers.

activate the RyR1 $Ca^{2+}$ release channel by itself (23–25,31), and to hypersensitize the channel for its activation by pharmacological agonists such as caffeine (26). Here we show that DP4 also increases the effectiveness of the DHPR transverse tubule voltage sensor to activate the RyR during depolarization of whole-cell, voltage-clamped adult skeletal muscle fibers.

The central domain of RyR1 contains mutations for both malignant hyperthermia (MH) and central core disease (26,45–49). Malignant hyperthermia is a dangerous hypermetabolic state after anesthesia with suxamethonium and/or volatile halogenated anesthetic agents (28). Studies on the $Ca^{2+}$ release properties of RyR1 channels containing MH mutations expressed in nonmuscle cells (50), myotubes (27,51–53), and muscle fibers (54,55) as well as animal models of MH (27,30) and humans (28,29), demonstrated that these MH mutations cause channel hyperactivation and hypersensitization effects.

DP4 produced MH-like hyperactivation of the wild-type RyR channel as described above, whereas it produced virtually no additional effect on the MH mutant RyR1 channels (22). Furthermore, as was shown previously, and in this study as well, Mut-DP4 that has the R2458C MH mutation in it produces no hyperactivation or hypersensitization effects.

Previous work in mechanically peeled skeletal muscle has shown that DP4 enhanced the force response to caffeine and to submaximal depolarization by change in ionic composition of the bathing solution, but that DP4 had no effect on the force response elicited by single AP (31). In particular, the influence of DP4 on depolarization-evoked $Ca^{2+}$ release has not been evaluated in adult whole-cell, voltage-clamped skeletal fibers. Here we first demonstrate that in murine voltage-clamped fibers, DP4 increases the amplitude of depolarization-induced $Ca^{2+}$ release without appreciably altering either its voltage-dependence or the kinetic properties of initial phase of the $Ca^{2+}$ release flux. DP4 induced an enhancement of ~64% on depolarization-evoked $Ca^{2+}$ release, thus confirming previous findings (23–25,31) regarding the potentiating effects of DP4 on $Ca^{2+}$ release, but here using voltage-clamp depolarization-evoked $Ca^{2+}$ release.

We also used the AP voltage-clamp technique simultaneously with high-speed confocal measurement of fluorescent $Ca^{2+}$ transients to establish that DP4 enhances AP-evoked $Ca^{2+}$ release. The difference between our results and a previous study (31) may reflect differences in methodology (skinned versus whole-cell voltage-clamped) and/or species differences (mouse versus rat). One disadvantage common to both the skinned fiber preparation and the whole-cell patch-clamp techniques is the potential loss of important intracellular constituents (34,56,57)—a process that could be faster in the skinned fiber preparation, and one which might explain the difference between these studies.

We also searched for potential effects of DP4 on the voltage-sensing machinery of the E-C coupling by measuring nonlinear capacitive currents to evaluate the properties of intramembrane charge movement. Interestingly, DP4 did not modify either the amplitude or the voltage dependence of the intramembrane charge movement, indicating that the voltage sensor machinery required for the activation of both RyR $Ca^{2+}$ release and DHPR $Ca^{2+}$ current (2–4,6) was not modified by this treatment. One striking observation was that DP4 also increased (24%) the maximum $Ca^{2+}$ conductance ($G_{max}$) without affecting either the voltage-dependence or the steepness of the $Ca^{2+}$ conductance versus voltage relationship. In contrast, application of 100 $\mu$M of Mut-DP4, a peptide identical to DP4 except for an R-2458-C mutation, had no appreciable effect on either depolarization-evoked $Ca^{2+}$ release or L-type $Ca^{2+}$ currents.

Our results demonstrate that in voltage-clamped fibers, DP4 induces two main effects on E-C coupling. The first effect is to sensitize final steps of orthograde E-C coupling. In this case, the effect of DP4 is to enhance depolarization-evoked $Ca^{2+}$ release via a direct regulation of RyR1 $Ca^{2+}$ release channel without affecting the voltage-sensing machinery of the DHPR. This effect is believed to be mediated by DP4 competing with its corresponding endogenous domain within RyR1 for binding to its complimentary N-terminal domain binding site within RyR1 (18,24,25), thereby destabilizing intramolecular signal-conduction pathway of the RyR1 and sensitizing activation of orthograde E-C coupling. Our results are consistent with the hypothesis that conformational changes in the DHPR T-tubule voltage sensor (5–7) and those in the RyR1 domain switch, which has been suggested to represent a putative channel regulatory domain (18,21,22,24,25), are tightly coupled. Thus, any mechanisms that reduce the energy barrier to destabilize tight interaction between the N-terminal domain and central domain, such as the presence of DP4, would facilitate turning the domain switch from off-position to on-position.

The second effect of DP4 on E-C coupling is possibly mediated by retrograde signaling between the RyR1 and L-type $Ca^{2+}$ channels. This form of signaling may induce an L-type channel state(s) with a higher open probability, perhaps the result of longer openings or shorter closed times (58), which in turn translates into enhanced $Ca^{2+}$ entry. Because of the lack of effect of DP4 on the voltage dependence of the charge movement or the $Ca^{2+}$ conductance, the augmentation on $G_{max}$ may arise from transitions that do not involve or require small charge movement (59). Whether this effect is a consequence of direct retrograde signaling or the result of a $Ca^{2+}$-dependent process (i.e., calmodulin-mediated $Ca^{2+}$-dependent facilitation) remains to be determined.

## CONCLUSIONS

Our results provide what we believe to be new information about the effects of DP4, a peptide derived from the central

domain of the RyR1, on orthograde and retrograde E-C coupling. Our results also suggest the hypothesis that DP4 can alter the intramolecular transduction of the activation signal within the RyR1, as well as the molecular communication from RyR1 to the skeletal muscle L-type $Ca^{2+}$ channel. It is clear that future studies are needed and that they will require detailed structural and molecular studies to identify the exact location(s) and interactions between critical regulatory domains in both DHPR and RyR1 as well as the exact functional consequences of such interactions. Overall, this domain peptide approach can be used as a tool to modulate and further study bidirectional signaling between DHPR-RyRs in skeletal muscle.

## SUPPORTING MATERIAL

Additional Materials and Methods are available at http://www.biophysj.org/biophysj/supplemental/S0006-3495(11)00421-8.

The project described was supported by grant No. RO1 AR055099 from the National Institute of Arthritis and Musculoskeletal and Skin Diseases, National Institutes of Health. R.O.O. was supported by National Institute of Arthritis and Musculoskeletal and Skin Diseases training grant No. T32 AR007592 to the Interdisciplinary Program in Muscle Biology, University of Maryland School of Medicine.

## REFERENCES

1. Horowicz, P., and M. F. Schneider. 1981. Membrane charge movement in contracting and non-contracting skeletal muscle fibers. *J. Physiol.* 314:565–593.
2. Huang, C. L. 1988. Intramembrane charge movements in skeletal muscle. *Physiol. Rev.* 68:1197–1247.
3. Ríos, E., and G. Pizarro. 1991. Voltage sensor of excitation-contraction coupling in skeletal muscle. *Physiol. Rev.* 71:849–908.
4. Schneider, M. F., and W. K. Chandler. 1973. Voltage dependent charge movement of skeletal muscle: a possible step in excitation-contraction coupling. *Nature.* 242:244–246.
5. Nakai, J., T. Tanabe, …, K. G. Beam. 1998. Localization in the II-III loop of the dihydropyridine receptor of a sequence critical for excitation-contraction coupling. *J. Biol. Chem.* 273:24983–24986.
6. Rios, E., and G. Brum. 1987. Involvement of dihydropyridine receptors in excitation-contraction coupling in skeletal muscle. *Nature.* 325: 717–720.
7. Tanabe, T., K. G. Beam, …, S. Numa. 1990. Regions of the skeletal muscle dihydropyridine receptor critical for excitation-contraction coupling. *Nature.* 346:567–569.
8. Nakai, J., R. T. Dirksen, …, P. D. Allen. 1996. Enhanced dihydropyridine receptor channel activity in the presence of ryanodine receptor. *Nature.* 380:72–75.
9. Nakai, J., N. Sekiguchi, …, K. G. Beam. 1998. Two regions of the ryanodine receptor involved in coupling with L-type $Ca^{2+}$ channels. *J. Biol. Chem.* 273:13403–13406.
10. Protasi, F., C. Paolini, …, P. D. Allen. 2002. Multiple regions of RyR1 mediate functional and structural interactions with $\alpha$(1S)-dihydropyridine receptors in skeletal muscle. *Biophys. J.* 83:3230–3244.
11. Sheridan, D. C., H. Takekura, …, C. F. Perez. 2006. Bidirectional signaling between calcium channels of skeletal muscle requires multiple direct and indirect interactions. *Proc. Natl. Acad. Sci. USA.* 103:19760–19765.
12. Berchtold, M. W., H. Brinkmeier, and M. Müntener. 2000. Calcium ion in skeletal muscle: its crucial role for muscle function, plasticity, and disease. *Physiol. Rev.* 80:1215–1265.
13. Divet, A., S. Paesante, …, F. Zorzato. 2005. Novel sarco(endo)plasmic reticulum proteins and calcium homeostasis in striated muscles. *J. Muscle Res. Cell Motil.* 26:7–12.
14. Prosser, B. L., N. T. Wright, …, M. F. Schneider. 2008. S100A1 binds to the calmodulin-binding site of ryanodine receptor and modulates skeletal muscle excitation-contraction coupling. *J. Biol. Chem.* 283:5046–5057.
15. Treves, S., M. Vukcevic, …, F. Zorzato. 2009. Minor sarcoplasmic reticulum membrane components that modulate excitation-contraction coupling in striated muscles. *J. Physiol.* 587:3071–3079.
16. Wright, N. T., B. R. Cannon, …, D. J. Weber. 2009. S100A1: structure, function, and therapeutic potential. *Curr. Chem. Biol.* 3:138–145.
17. Samsó, M., W. Feng, …, P. D. Allen. 2009. Coordinated movement of cytoplasmic and transmembrane domains of RyR1 upon gating. *PLoS Biol.* 7:e85.
18. Ikemoto, N., and T. Yamamoto. 2002. Regulation of calcium release by interdomain interaction within ryanodine receptors. *Front. Biosci.* 7:d671–d683.
19. Kobayashi, S., M. L. Bannister, …, N. Ikemoto. 2005. Dantrolene stabilizes domain interactions within the ryanodine receptor. *J. Biol. Chem.* 280:6580–6587.
20. Bannister, M. L., T. Hamada, …, N. Ikemoto. 2007. Malignant hyperthermia mutation sites in the $Leu^{2442}$-$Pro^{2477}$ (DP4) region of RyR1 (ryanodine receptor 1) are clustered in a structurally and functionally definable area. *Biochem. J.* 401:333–339.
21. Kobayashi, S., T. Yamamoto, …, N. Ikemoto. 2004. Antibody probe study of $Ca^{2+}$ channel regulation by interdomain interaction within the ryanodine receptor. *Biochem. J.* 380:561–569.
22. Murayama, T., T. Oba, …, Y. Ogawa. 2007. Postulated role of interdomain interaction between regions 1 and 2 within type 1 ryanodine receptor in the pathogenesis of porcine malignant hyperthermia. *Biochem. J.* 402:349–357.
23. Shtifman, A., C. W. Ward, …, M. F. Schneider. 2002. Interdomain interactions within ryanodine receptors regulate $Ca^{2+}$ spark frequency in skeletal muscle. *J. Gen. Physiol.* 119:15–32.
24. Yamamoto, T., R. El-Hayek, and N. Ikemoto. 2000. Postulated role of interdomain interaction within the ryanodine receptor in Ca(2+) channel regulation. *J. Biol. Chem.* 275:11618–11625.
25. Yamamoto, T., and N. Ikemoto. 2002. Spectroscopic monitoring of local conformational changes during the intramolecular domain-domain interaction of the ryanodine receptor. *Biochemistry.* 41:1492–1501.
26. Betzenhauser, M. J., and A. R. Marks. 2010. Ryanodine receptor channelopathies. *Pflugers Arch.* 460:467–480.
27. Chelu, M. G., S. A. Goonasekera, …, S. L. Hamilton. 2006. Heat- and anesthesia-induced malignant hyperthermia in an RyR1 knock-in mouse. *FASEB J.* 20:329–330.
28. Denborough, M. A., J. F. Forster, …, J. D. Villiers. 1962. Anaesthetic deaths in a family. *Br. J. Anaesth.* 34:395–396.
29. Melzer, W., and B. Dietze. 2001. Malignant hyperthermia and excitation-contraction coupling. *Acta Physiol. Scand.* 171:367–378.
30. Mickelson, J. R., and C. F. Louis. 1996. Malignant hyperthermia: excitation-contraction coupling, $Ca^{2+}$ release channel, and cell $Ca^{2+}$ regulation defects. *Physiol. Rev.* 76:537–592.
31. Lamb, G. D., G. S. Posterino, …, N. Ikemoto. 2001. Effects of a domain peptide of the ryanodine receptor on $Ca^{2+}$ release in skinned skeletal muscle fibers. *Am. J. Physiol. Cell Physiol.* 281:C207–C214.
32. Liu, Y., S. L. Carroll, …, M. F. Schneider. 1997. Calcium transients and calcium homeostasis in adult mouse fast-twitch skeletal muscle fibers in culture. *Am. J. Physiol.* 272:C1919–C1927.
33. Prosser, B. L., E. O. Hernández-Ochoa, …, M. F. Schneider. 2009. The Qgamma component of intra-membrane charge movement is present in mammalian muscle fibres, but suppressed in the absence of S100A1. *J. Physiol.* 587:4523–4541.

34. Hamill, O. P., A. Marty, …, F. J. Sigworth. 1981. Improved patch-clamp techniques for high-resolution current recording from cells and cell-free membrane patches. *Pflugers Arch.* 391:85–100.

35. Wang, Z. M., M. L. Messi, and O. Delbono. 1999. Patch-clamp recording of charge movement, $Ca^{2+}$ current, and $Ca^{2+}$ transients in adult skeletal muscle fibers. *Biophys. J.* 77:2709–2716.

36. Starzak, M. E., and R. J. Starzak. 1978. An action potential clamp to probe the effectiveness of space clamp in axons. *IEEE Trans. Biomed. Eng.* 25:201–204.

37. Prosser, B. L., E. O. Hernández-Ochoa, …, M. F. Schneider. 2009. Simultaneous recording of intramembrane charge movement components and calcium release in wild-type and S100A1-/- muscle fibres. *J. Physiol.* 587:4543–4559.

38. Klein, M. G., B. J. Simon, …, M. F. Schneider. 1988. Simultaneous recording of calcium transients in skeletal muscle using high- and low-affinity calcium indicators. *Biophys. J.* 53:971–988.

39. Royer, L., S. Pouvreau, and E. Ríos. 2008. Evolution and modulation of intracellular calcium release during long-lasting, depleting depolarization in mouse muscle. *J. Physiol.* 586:4609–4629.

40. Shirokova, N., J. García, …, E. Ríos. 1996. $Ca^{2+}$ release from the sarcoplasmic reticulum compared in amphibian and mammalian skeletal muscle. *J. Gen. Physiol.* 107:1–18.

41. Schneider, M. F., and B. J. Simon. 1988. Inactivation of calcium release from the sarcoplasmic reticulum in frog skeletal muscle. *J. Physiol.* 405:727–745.

42. Schneider, M. F., B. J. Simon, and G. Szucs. 1987. Depletion of calcium from the sarcoplasmic reticulum during calcium release in frog skeletal muscle. *J. Physiol.* 392:167–192.

43. Harkins, A. B., N. Kurebayashi, and S. M. Baylor. 1993. Resting myoplasmic free calcium in frog skeletal muscle fibers estimated with fluo-3. *Biophys. J.* 65:865–881.

44. Baylor, S. M., and S. Hollingworth. 2010. Calcium indicators and calcium signaling in skeletal muscle fibres during excitation-contraction coupling. *Prog. Biophys. Mol. Biol.* 105:162–179.

45. Barone, V., O. Massa, …, V. Sorrentino. 1999. Mutation screening of the RYR1 gene and identification of two novel mutations in Italian malignant hyperthermia families. *J. Med. Genet.* 36:115–118.

46. Brandt, A., L. Schleithoff, …, F. Lehmann-Horn. 1999. Screening of the ryanodine receptor gene in 105 malignant hyperthermia families: novel mutations and concordance with the in vitro contracture test. *Hum. Mol. Genet.* 8:2055–2062.

47. Chamley, D., N. A. Pollock, …, R. L. Brown. 2000. Malignant hyperthermia in infancy and identification of novel RYR1 mutation. *Br. J. Anaesth.* 84:500–504.

48. Manning, B. M., K. A. Quane, …, T. V. McCarthy. 1998. Novel mutations at a CpG dinucleotide in the ryanodine receptor in malignant hyperthermia. *Hum. Mutat.* 11:45–50.

49. Rueffert, H., D. Olthoff, …, U. G. Froster. 2004. A new mutation in the skeletal ryanodine receptor gene (RYR1) is potentially causative of malignant hyperthermia, central core disease, and severe skeletal malformation. *Am. J. Med. Genet. A.* 124A: 248–254.

50. Tong, J., H. Oyamada, …, D. H. MacLennan. 1997. Caffeine and halothane sensitivity of intracellular $Ca^{2+}$ release is altered by 15 calcium release channel (ryanodine receptor) mutations associated with malignant hyperthermia and/or central core disease. *J. Biol. Chem.* 272:26332–26339.

51. Bannister, R. A., E. Estève, …, K. G. Beam. 2010. A malignant hyperthermia-inducing mutation in RYR1 (R163C): consequent alterations in the functional properties of DHPR channels. *J. Gen. Physiol.* 135:629–640.

52. Dietze, B., J. Henke, …, W. Melzer. 2000. Malignant hyperthermia mutation $Arg^{615}Cys$ in the porcine ryanodine receptor alters voltage dependence of $Ca^{2+}$ release. *J. Physiol.* 526:507–514.

53. Yang, T., T. A. Ta, …, P. D. Allen. 2003. Functional defects in six ryanodine receptor isoform-1 (RyR1) mutations associated with malignant hyperthermia and their impact on skeletal excitation-contraction coupling. *J. Biol. Chem.* 278:25722–25730.

54. Andronache, Z., S. L. Hamilton, …, W. Melzer. 2009. A retrograde signal from RyR1 alters DHP receptor inactivation and limits window $Ca^{2+}$ release in muscle fibers of Y522S RyR1 knock-in mice. *Proc. Natl. Acad. Sci. USA.* 106:4531–4536.

55. Owen, V. J., N. L. Taske, and G. D. Lamb. 1997. Reduced $Mg^{2+}$ inhibition of $Ca^{2+}$ release in muscle fibers of pigs susceptible to malignant hyperthermia. *Am. J. Physiol.* 272:C203–C211.

56. Allen, D. G., G. D. Lamb, and H. Westerblad. 2008. Skeletal muscle fatigue: cellular mechanisms. *Physiol. Rev.* 88:287–332.

57. Fenwick, E. M., A. Marty, and E. Neher. 1982. Sodium and calcium channels in bovine chromaffin cells. *J. Physiol.* 331:599–635.

58. Hess, P., J. B. Lansman, and R. W. Tsien. 1984. Different modes of Ca channel gating behavior favored by dihydropyridine Ca agonists and antagonists. *Nature.* 311:538–544.

59. Bezanilla, F. 2000. The voltage sensor in voltage-dependent ion channels. *Physiol. Rev.* 80:555–592.